Results in Optics 16 (2024) 100695

Contents lists available at ScienceDirect

Results in Optics

journal homepage: www.elsevier.com/locate/rio

Polarization-resolved near-field characterization of coupling between a bus waveguide and a ring resonator

V.V. Tkachuk [a,*], J.P. Korterik [a], L. Chang [b], H.L. Offerhaus [a]

[a] Optical Sciences group, MESA+ research institute, University of Twente, The Netherlands
[b] Integrated Optical Systems group, MESA+ research institute, University of Twente, The Netherlands

ARTICLE INFO

Keywords:
SNOM
NSOM
Evanescent field
Ring resonators

ABSTRACT

Light propagation in Photonic integrated circuits (PICs), which can nowadays involve complex systems of light-guiding structures, is measured with different approaches(Nuzhdin et al., 2020, Lončar et al., 2002, Hopman et al., 2007, Morichetti et al., 2014, Sapienza et al., 2012, Vesseur et al., 2007). An interferometric polarization-sensitive measurement of the evanescent fields of these structures provides insight in the performance of the circuit detects possible malfunction with sub-wavelength precision(Engelen et al., 2007, Gersen et al., 2005, Barwick et al., 2009). We demonstrate a Near-field scanning optical microscopy (NSOM) measurement on coupled ring resonators that shows how the guided modes evolve as they propagate across the optical chip. Analysis of the measurements provides information about intensity distribution of the two polarization components (TE and TM) and their spatial confinement. The data validates our methodology and opens new possibilities for analysis of signal propagation in prototyping and optimization of integrated optical systems. Direct observation of polarization state of the guided modes allows for clear understanding of mode conversion in coupling systems.

1. Introduction

Photonic integrated circuits consist of building blocks, such as tapers, straight waveguides, junctions, couplers and resonators. Their use allows numerous applications in optical communication and processing units.

In photonic structures with microscopic dimensions, the electromagnetic field distribution is described in terms of approximated Maxwell's equations. Commonly, only the persisting, propagating field distributions are examined (Iluz et al., 2024). These propagating modes are characterized by a fast oscillation of the phase and a relatively slow decay of the envelope. Generally, they are described in terms of a complex wave vector k, where the real part corresponds to the oscillation of the phase and the imaginary part represents the loss. Multi-mode waveguides support a number of such modes with different polarization states (known as TE- and TM-modes).

Measuring the local optical phase and amplitude inside integrated optical structures with a Near-Field Optical Microscope (NSOM) provides a detailed understanding of the propagation of the excited light inside. It presents the researchers with an almost direct way of observation of the total sum of guided waveguide modes. A restriction of the near field method is the requirement to access the evanescent wave around the waveguide which limits the possibilities for a cladding on the waveguide to sub-micron cladding thicknesses.

Holding the sample steady and allowing for precise maneuvering is vital for high-quality NSOM imaging. There are two main ways of positioning the sample with respect to the objective lens in the system: on- and off-axis, also commonly referred to as (sample-)vertical and horizontal arrangement (Fig. 2). The key difference in these arrangements is the sample and probe alignment procedure. In case of the off-axis (horizontal) arrangement (Fig. 2, bottom), the sample has to be positioned with respect to the lens first, then the probe has to be brought in the vicinity of the sample. This accommodates end-facet coupling method of inspection of light-guiding structures, where the exclusion of stray light is of utmost importance. In case of the coaxial (vertical) arrangement (Fig. 2, top), the lens and probe can be aligned first, and the sample may then be brought between them. This method is most suitable for observation of regular samples and photonic structures which have to be illuminated from the backside.

Depending on the exact arrangement and type of the illumination and detection, NSOM can operate in several modes (Fig. 1), each of them providing unique experimental approach to near-field measurement (Courjon, 2003; Zayats and Richards, 2009).

* Corresponding author.
E-mail address: v.tkachuk@utwente.nl (V.V. Tkachuk).

https://doi.org/10.1016/j.rio.2024.100695
Received 5 January 2024; Received in revised form 31 March 2024; Accepted 19 May 2024
Available online 25 May 2024

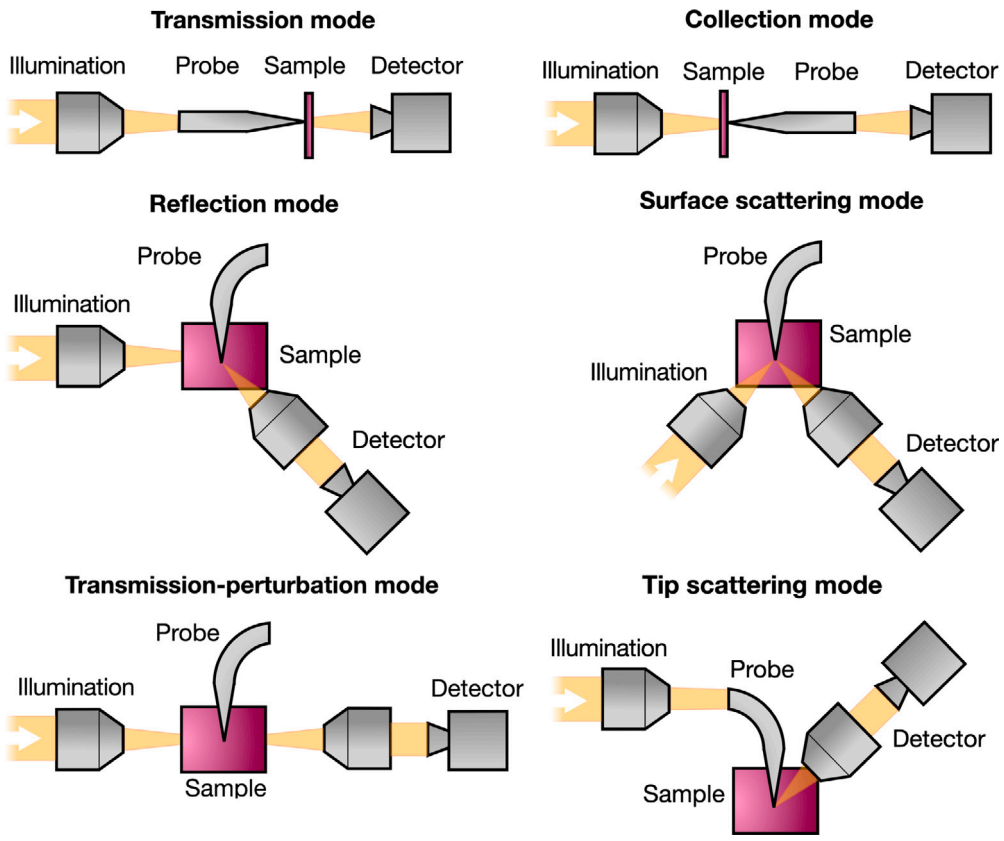

Fig. 1. Schematic illustration of main NSOM modes.

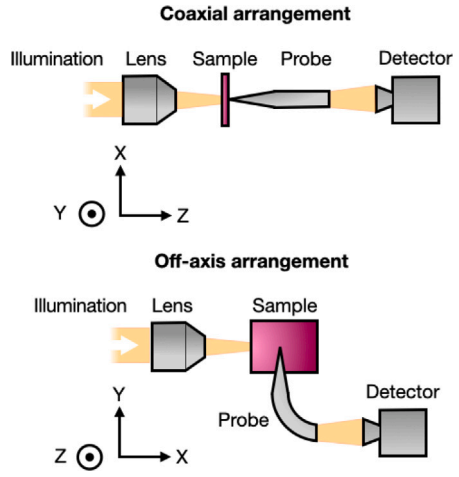

Fig. 2. Schematic representation of two main NSOM arrangements with respect to incoming laser beam. Note that the coordinate system is oriented with the sample. Coaxial arrangement is realized in Dikken (2015) and Higgins et al. (1996). Off-axis arrangement is realized in le Feber (2015) and this work.

Photonic integrated ring resonators are a commonly employed building block in the field of integrated optics, which utilizes the principles of light confinement and resonance to perform a variety of optical functions. Consisting of a closed loop that guides light, allowing the light to circulate multiple times. This process amplifies certain wavelengths of light through constructive interference. The interference causes the device to selectively enhance or suppress certain wavelengths. The resonance condition of a ring resonator is determined by its circumference, the refractive index, and the wavelength of the light, fulfilling the condition where the optical path length is an integer multiple of the wavelength. Optical filtering and multiplexing, sensors, modulators and switches utilize the high sensitivity of the ring resonators to manipulate light in a controlled manner (Bogaerts et al., 2012).

The idea of simultaneous heterodyne detection of perpendicular polarization components was implemented earlier (Dikken, 2015). However is was only applied to samples where the two polarization directions were perpendicular to the probe (Fig. 2). In such a system, the alignment can be done before the sample is inserted. This approach, while making the alignment and scanning easier, does not accommodate for scanning end facet-coupled optical chips.

An alternative scheme was realized and discussed by le Feber (2015) and Rotenberg et al. (2015), where the interference was confined to a fiber splitter. This greatly simplifies the alignment, but compromises the ability to control the interferometer arms independently to ensure maximum extinction between the orthogonal polarizations, which is required for low-signal measurements on waveguides and resonators. Yet another approach with a modulated polarization in an illumination NSOM was also previously realized (Higgins et al., 1996).

The aforementioned adaptation to the setup unveil its potential in polarization-resolved chip-scale large area scanning, which, to the knowledge of the authors, was not published before. Significant advances were made in the development of NSOM techniques in previous decades. Abashin et al. (2006) demonstrated the application of Fourier analysis to distinguishing the propagating modes in a Silicon photonic crystal waveguide using a similar setup. In a recent work, Pin et al. emphasized the importance of applications of studying the quasi-interference of guided modes in waveguides by applying them to achieve optical tweezing (Pin et al., 2018). In this paper, we continue the investigation into the properties of propagating modes by analyzing the difference in propagation loss between several modes supported in the waveguide.

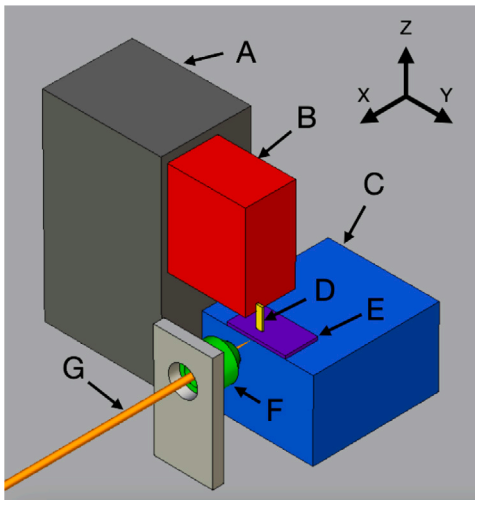

Fig. 3. Schematic representation of the scanning part of NSOM. A – Scanning head positioning (contains encoded motors for coarse probe positioning). B – Scanning head (contains piezo-actuators for scanning the probe) C – Sample holder (contains stick–slip motors for sample alignment). D – Probe. E – Sample. F – In-coupling lens. G – Laser beam.

2. Concept of operation and experimental arrangement

2.1. NSOM

On the outside of a waveguide, a propagating light waves give rise to an evanescent field, which decays exponentially away from the interface but can be picked up by the sub-wavelength aperture of the NSOM. This is made possible by local conversion of the evanescent wave near the surface of the waveguide into a propagating wave inside the fiber probe. This light is can be detected more efficiently by means of heterodyne detection. Depending on the thickness of the waveguide, the evanescent field, picked up by the probe, represents a combination of all the modes present in the waveguide in the vicinity of the probe. The relative strength of different modes in the detected signal is not directly representative of their relative strength inside the photonic structures since different modes have different evanescent fields. However, if the tip remains at a constant distance, the fractions that are picked up can be considered constant.

A core advantage of the NSOM technique lies in ability to accurately measure the local behavior of the light waves inside photonic structures. It also allows for probing of segments of the waveguide without destroying the waveguide. Lastly, the measurements are not subject to diffraction limit of detection for the scattered light, unlike in conventional far-field optical microscopy.

Because the span of a scanning field of the typical scanning probe microscope is limited by the deflection of the piezo-actuator(s) (Fig. 3), consecutive measurements across macroscopic distances require moving either the whole scanning head over the sample, or the sample under the scanning head. For an NSOM in collection mode, the former is much more practical because the latter requires the coupling of the light onto the chip to be moved. For the purpose of this research, the scanning head of an NSOM was outfitted with a three-dimensional course positioning stage, thus allowing automated positioning across 25 mm in each direction.

Compared to previous publications (Dikken, 2015), the shear-force feedback system underwent considerable revision. The instability of the set-point signal from the scanning head's pre-amplifier, when the tuning fork was shaken mechanically to allow shear-force detection, was a hindrance to continuous scanning because of need of frequently adjusting the error signal between consecutive scans. Moreover, the movement of the scanning head across larger distances introduced additional factors compromising the stability of the frequency-amplitude response of the system. To combat that, a fully electronic actuation method was introduced in the system along with a new, rigorously selected pre-amplifier. The results of that study are published in Tkachuk et al. (2023).

As the light source, Toptica DL pro was used to operate at 970 nm. The system was tuned for single-mode operation across different power levels.

The light was coupled in the sample by using a coarse manual adjustment of the sample table against a lens-equipped camera, sensitive to both visible and near-infrared light, set coaxial to the in-coupling laser beam was near the waveguide under treatment. Following that, a more accurate positioning was performed using three-axis piezoelectric stick–slip motor system. The movement was referenced against another camera, set at an angle in a way to both image the light coming from the waveguide as well as the tip of the fiber, which is later brought in contact to the illuminated waveguide at the desired location.

A detailed description of the NSOM used in this investigation is given in Appendix. The principle scheme is depicted in Fig. 4. The detection of differently polarized guided modes to evanescent field, and following polarization-resolved detection of the evanescent field by the probe is explained in Fig. 5. The lower $\lambda/2$ and $\lambda/4$ plate compensate the birefringence in the probe and fiber. Because of the direction of propagation of guided modes in the waveguide, one detector will receive signal from both the TE- and TM-modes in the waveguide, while the other detector will receive signal predominantly from TM-modes.

Different modes in the Aluminum Oxide (Al_2O_3) on Silicon Oxide (SiO_2) waveguides are excited by a laser at 970 nm wavelength. The waveguide is scanned with the near-field probe over several segments. In the overall detected signal (two channels for the polarization states respectively), we extract the different modes by means of Fourier analysis. This information is used to derive the different propagation constants and explain the difference in propagation loss between the modes. This study reveals the reproducibility and precision with which the polarization-resolved mode analysis can be done on waveguides using NSOM.

2.2. Sample description

An optical microscopy photograph (Fig. 7, A) shows the layout of the fabricated device, consisting of a straight waveguide with tapering and a ring resonator. The geometrical parameters are as follows: total length ≈2 cm, width 1.5 μm, height ≈450 nm. The total length of the straight segment is about 9 mm. The ring radius is 175 μm. The device is fabricated on a thermally oxidized silicon wafer. A 450 nm Al_2O_3 oxide layer was deposited using reactive sputter deposition on top of 8 μm polished SiO_2. The structures were defined using electron beam lithography with a negative e-beam resist, followed by reactive ion etching.

To facilitate the injection of the light into the device, the waveguides are tapered towards the input facets. This taper (starting width 12 μm) performs an adiabatic mode conversion to 1.6-μm width to better match the mode profile of the waveguide. PECVD SiO_2 top cladding is deposited on the input coupling taper region, but not on top of the micro ring.

The expected mode profile of this waveguide (with air top cladding) is simulated using numerical, Ansys Lumerical Finite-Difference Eigenmode (FDE), and experimental data obtained during the fabrication process. The results of the modeling are summarized in Table 1. We use the experimentally determined values of the first and second supported TE modes to confirm their effective refractive index (1.56 and 1.47 respectively). The first and second supported TM modes also match the simulation data (1.52 and 1.45 respectively). Using discrete Fourier transfer, we can estimate the n_{eff} of the guided modes in the straight bus waveguide, however, estimating n_{eff} in curved (ring) structure remains a challenging task and is not further explored in this study.

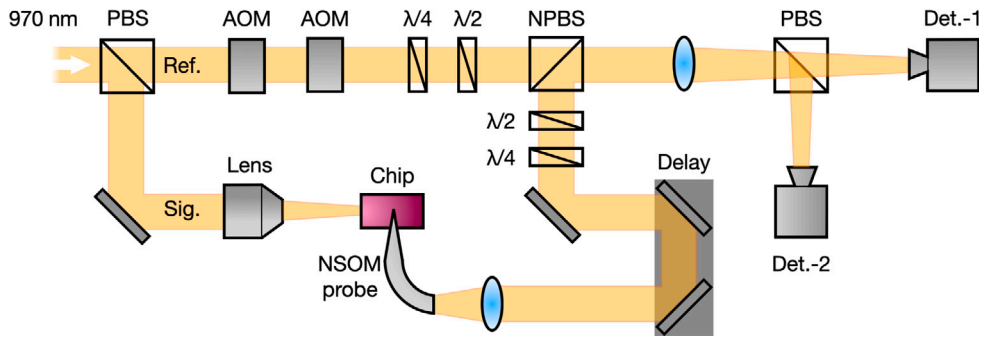

Fig. 4. Schematic representation of the polarization-sensitive NSOM configured in collection mode for investigation of propagation of light inside the photonic integrated chip. A combination of two AOMs shifts the frequency of light in the reference branch by 100 kHz. $\lambda/4$ plates ensure that the light in each branch is linearly polarized before hitting the PBS, and $\lambda/2$ plates allow distributing the polarizations between the detectors.

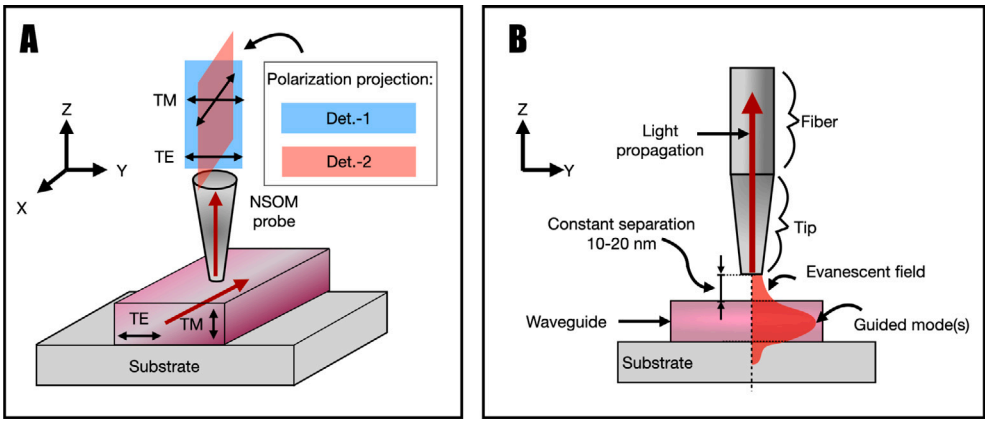

Fig. 5. Schematic representation of detection of the orthogonal modes during the NSOM scanning. A – The propagation axes convention used in the work. B – a detailed depiction imaging of the evanescent field by the near-field probe. Note that the detected TE/TM signal is not necessarily the same as TE/TM guided modes in the waveguide since the coupling coefficients can vary.

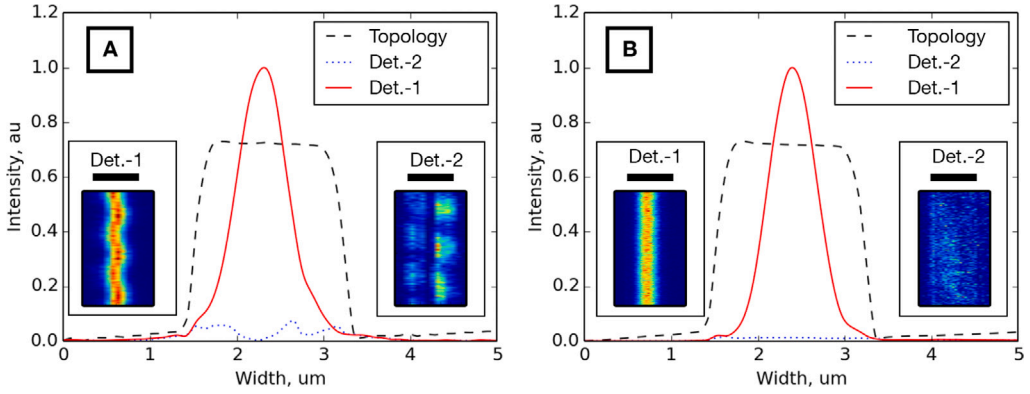

Fig. 6. Topology and intensity profiles of the single-mode waveguide. The inserts depict the 2D intensity profiles, all normalized between the values of 0 and 1 for better visibility. The height of the waveguide is 450 nm (data from inter-process measurement). A – with the optical feedback from the ring. B – without the optical feedback from the ring, with ratio of peak intensity of (1:0.05). The scale bar represents the width of the waveguide, 1.5 μm.

Table 1
Results of the numerical study of the waveguide at 970 nm.

Mode	Effective index	TE polarization fraction (Ex)	Waveguide TE/TM fraction (%)	Effective area (μm^2)
TE_{00}	1.564	100	96.57/91.59	0.671
TM_{00}	1.527	0	87.97/97.47	0.944
TE_{01}	1.476	99	87.46/92.65	0.899
TM_{01}	1.454	1	90.37/90.49	1.147

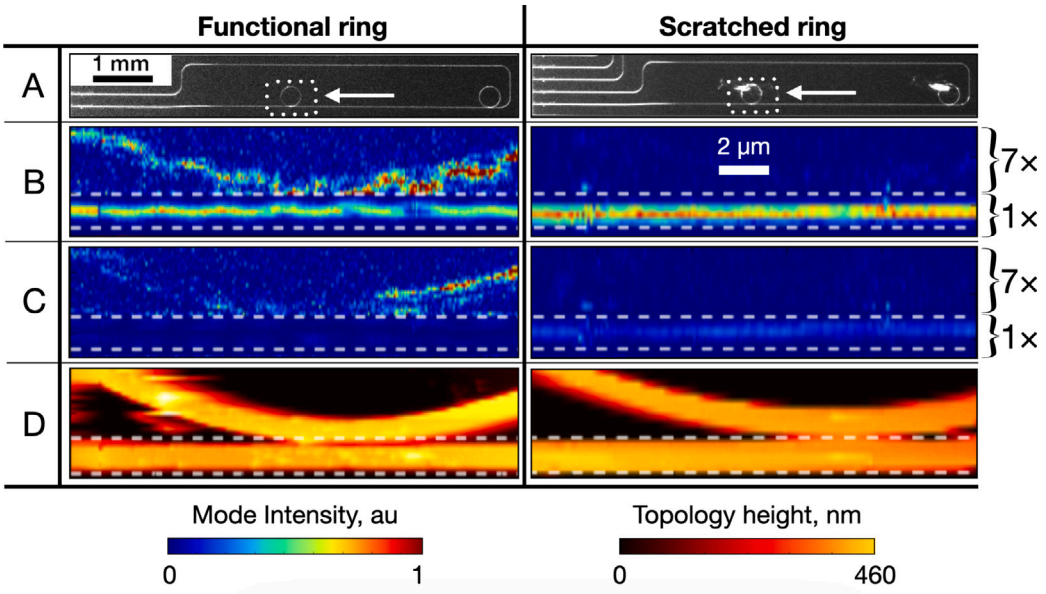

Fig. 7. A – optical image. B,C – optical intensity of the coupled waveguide-ring system captured by Det.-1 (B) and Det.-2. The amplitude of signal is amplified 7× outside of the waveguide for better visibility, as denoted by the corresponding brackets. (C). D – topology image of the coupled waveguide-ring system. B-D are to scale. Note that the geometric profile of the waveguide is slightly distorted due to the geometry of the probe and dynamic behavior of the height feedback system.

3. Results and discussion

Linearly polarized (TE-like) light was coupled in the chip. The polarization state was purified by a Glenn-Taylor polarizer, set in the beam path right before the in-coupling lens.

For the linear (TE-like) input, the fundamental TE_{00} mode will be predominantly excited in the bus waveguide and consequently captured by the Det.-1 (Fig. 6, B). This is evident from the calculated n_{eff}: for TE_{00} 1.56, TM_{00} 1.54, and TE_{01} 1.47± 0.02 correspondingly, which corresponds well to the values found in Table 1. The accuracy of this measurement is mainly contingent upon the physical length of the scan, and cannot be improved by scanning with higher spatial resolution. Transitions like coupling can also excite other modes which will create interference. The spatial pattern can reveal the type of mode that is interfering. The TM modes will also be present in the form of beating between TE and TM modes on the signal from Det. -1, since the signal from the TM modes is distributed over both detectors. Det.-2 will see only (half of) the TM modes in the waveguide.

When a ring resonator is coupled to the waveguide, it converts a portion of the fundamental modes to higher-order modes (Fig. 10, "Functional ring"). If, however, the ring is defect and light cannot resonate inside it, the guided modes in the bus waveguide experience no conversion, and, subsequently, no guided modes are injected back into the bus waveguide from the ring resonator (Fig. 10, "Scratched ring"). As the TE modes propagate along the ring, their polarization rotates with respect to polarization in the straight waveguide. In our configuration, we observe this as a transfer of the intensity from the Det.-1 to the Det.-2. The setup is adjusted to ensure equal sensitivity to the orthogonal polarizations and their linear polarization (Tkachuk et al., 2024). To confirm this, the half-wave plate, through which the light is coupled in the sample on the signal branch, was scanned between 0° and 90° relative to the polarization angle of the incoming signal, while the probe was held at the position of interference peak (Fig. 11). From the examination of this result, it is clear that the TE and TM-mode can be fully separated. The inherent scrambling of polarization state of the picked signal is compensated for externally. The exact process of conversion of the polarizations, which takes place in the aperture probe, is out of the scope of this study. Since the TM modes are distributed over both detectors, we do not observe the same

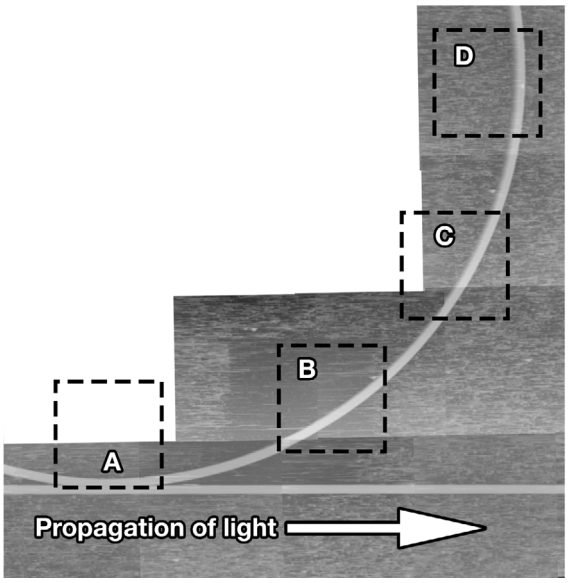

Fig. 8. Scanning probe microscopy image of the waveguide-ring system. A-D outline the areas where the intensity in Fig. 9 was measured.

transfer, and, after a quarter of the ring, Det.-1 shows only TM signal, while Det.-2 shows a combination of TE and TM.

Further scanning along the ring (from 90° on to the complete circle) demonstrates the same characteristic distribution of intensity, which serves as confirmation.

Introduction of an automated NSOM scanning routine allows obtaining the intensity along the ring in the rapid manner and thus minimize the time-resolved drift in the system (Fig. 8). After the phase-resolved NSOM scans of the ring segments are obtained, the scans can be unbent until the bent waveguide becomes straight, as observed in the topology image. Once the topology image is straightened, the same transformation can be applied to the optical image as well. After that, the intensity can be integrated along the waveguide by summing the intensity values and diving the result by the number of

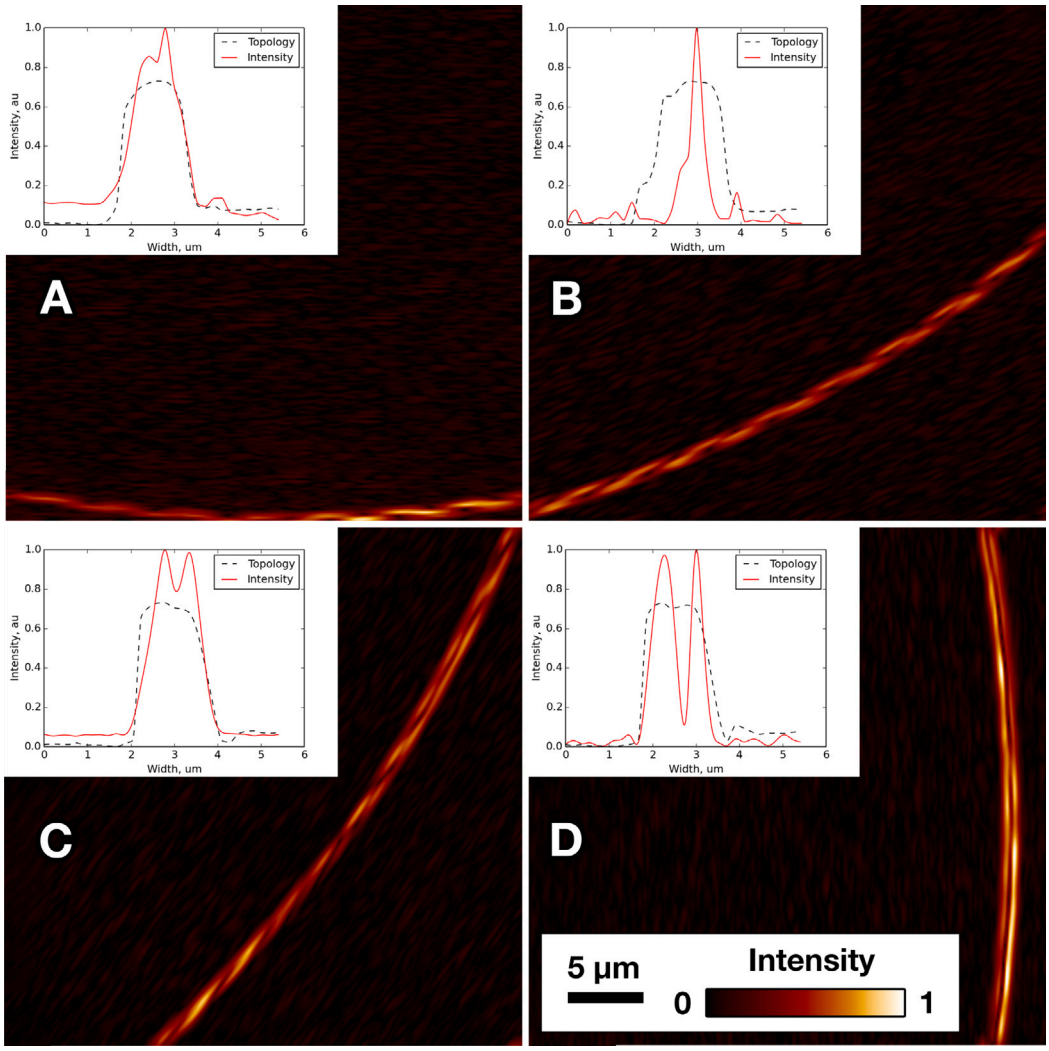

Fig. 9. Combined optical signal intensity of the indicated segments on the ring, as seen on Fig. 8, A-D. The inserts show the integrated intensity profiles with respect to the topology cross section in the scanned area.

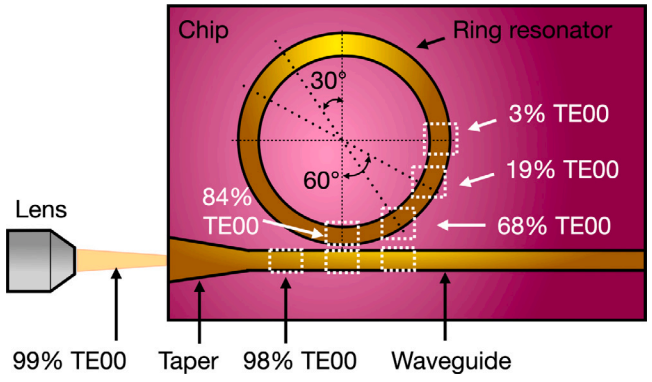

Fig. 10. Schematic representation of the measurement to resolve TE00 mode changing its polarization with respect to the Det.-1 signal.

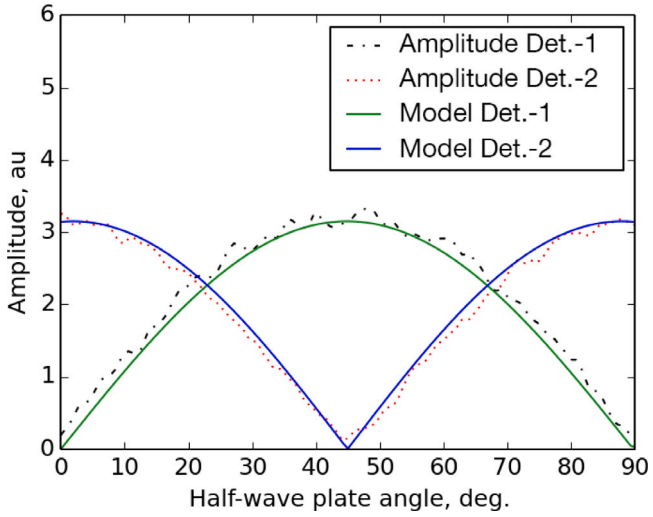

Fig. 11. Comparison between measurement and model of change amplitude on Det.-1 and Det.-2 as the half-wave plate is scanned between 0° and 90° relative to the polarization angle of the incoming signal.

summed pixels. This summation corresponds to the intensity picked up from the waveguide and presents a composition of Hermite–Gaussian modes (Saghafi and Sheppard, 1998), derived from the near field above the surface of the waveguide in which they are present. The results are shown in Fig. 9. In Fig. 9A It can be seen that some signal is detected in Det.-2 showing that a TM-mode has been excited. From the drop in

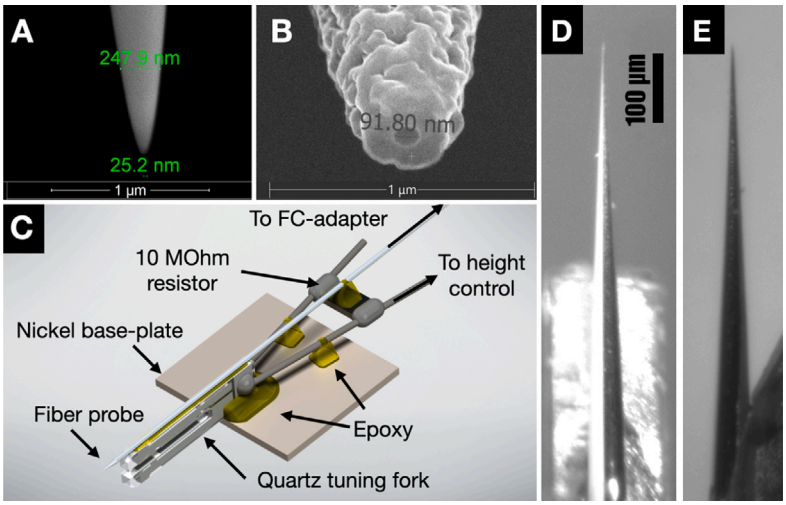

Fig. A.12. Interchangeable NSOM probe assembly. A – SEM image of a pulled fiber. B – SEM image of the aperture on the apex of the fiber. C – Assembly view of the probe. D (top-), E (side-view) – optical microscopy image of the tip of the fiber probe, with the tuning fork prong visible.

signal on Det.-1 going from 9A to B we can see that also a TE mode was excited, and, since the shape changes from a centralized peak to two lobes, it is likely that we excite a TE_{00} mode.

4. Conclusion

We have demonstrated polarization resolved characterization of propagation of different modes in a waveguide, coupling to a ring resonator. We extract the intensity profiles along the ring resonators and demonstrate that polarizations can be separated by compensating the birefringence of the probe fiber. This compensation remains stable for the duration of scanning, as long as the fiber does not change its overall shape, i.e. for days. With this new ability, PICs and their functionalities can be probed locally. Acquiring polarization state of the guided modes in coupled bus waveguide-ring systems allows the researchers to directly observe the mode conversion during the characterization of photonic structures, and determine the functionality of the photonic integrated devices.

CRediT authorship contribution statement

V.V. Tkachuk: Writing – review & editing, Writing – original draft, Visualization, Validation, Software, Resources, Methodology, Investigation,Formal analysis, Data curation, Conceptualization. **J.P. Korterik:** Writing – review & editing, Supervision, Resources. **L. Chang:** Writing – review & editing, Supervision. **H.L. Offerhaus:** Writing – review & editing, Supervision, Resources, Project administration.

Declaration of competing interest

The authors declare that they have no known competing financial interests or personal relationships that could have appeared to influence the work reported in this paper.

Data availability

Data will be made available on request.

Appendix. Description of the NSOM

NSOM has a disposable probe, construction of which is modified specially for the purpose of this study (Fig. A.12). To facilitate continuous measurement of one scanning field after another in shortest time possible, the amplitude-transfer characteristics of the probe, namely the resonance frequency and quality factor, should remain unaffected between several measurements. One of the significant changes to the assembly was to rely on the electronic excitation of the tuning fork, which alleviated problems with unwanted resonance peaks and overall mechanical stability. This means that the contacts of the tuning fork are now electrically isolated from the ground of the setup.

After the light is coupled in the waveguide, the fiber probe can be visually aligned with the area of interest (for example, the minimal distance between the waveguide and the ring resonator) visually based on the image form an optical microscope. This, in practice, allows landing the probe within 10 µm of the desired spot, limit to resolution of the optical microscope and amount of light reflected from the probe apex and the photonic structures.

If the scan area contains a straight waveguide, its position with respect to the scanning head can easily be predicted from two such scans, and extrapolated to position the probe anywhere on the waveguide. After scanning any extent segment of the ring, it is trivial to estimate the coordinates of the center of the ring and, hence, calculate the positions of any number of scan fields on the ring.

Within the limitations of the temporal stability of the probe assembly and the laser, a number of scan fields may then be queued up for scanning. The authors were thus able to scan as many as 52 overlapping scan fields covering a square of almost 0.45 mm, and 14 consecutive segments on a straight waveguide, covering over 1 mm, without need of changing any settings in the setup.

References

Abashin, M., Tortora, P., Märki, I., Levy, U., Nakagawa, W., Vaccaro, L., Herzig, H.P., Fainman, Y., 2006. Near-field characterization of propagating optical modes in photonic crystal waveguides. Opt. Express 14 (4), 1643–1657. http://dx.doi.org/10.1364/OE.14.001643.

Bogaerts, W., De Heyn, P., Van Vaerenbergh, T., De Vos, K., Kumar Selvaraja, S., Claes, T., Dumon, P., Bienstman, P., Van Thourhout, D., Baets, R., 2012. Silicon microring resonators. Laser Photonics Rev. 6 (1), 47–73. http://dx.doi.org/10.1002/lpor.201100017.

Courjon, D., 2003. Near-Field Microscopy and Near-Field Optics. World Scientific Publishing Company.

Dikken, D., 2015. Antennas for Light and Plasmons (Ph.D. thesis). University of Twente, Netherlands, http://dx.doi.org/10.3990/1.9789036539531.

Higgins, D.A., Vanden Bout, D.A., Kerimo, J., Barbara, P.F., 1996. Polarization-modulation near-field scanning optical microscopy of mesostructured materials. J. Phys. Chem. 100 (32), 13794–13803. http://dx.doi.org/10.1021/jp9609951.

Iluz, M., Cohen, K., Kheireddine, J., Hazan, Y., Rosenthal, A., Tsesses, S., Bartal, G., 2024. Unveiling the evolution of light within photonic integrated circuits. Optica 11 (1), 42. http://dx.doi.org/10.1364/OPTICA.504397.

le Feber, B., 2015. Nanoscale Electric and Magnetic Optical Vector Fields: Mapping and Injection (Ph.D. thesis). University of Twente, Netherlands, http://dx.doi.org/10.3990/1.9789462594913.

Pin, C., Jager, J.-B., Tardif, M., Picard, E., Hadji, E., Fornel, F., Cluzel, B., 2018. Optical tweezing using tunable optical lattices along a few-mode silicon waveguide. Lab Chip 18, http://dx.doi.org/10.1039/C8LC00298C.

Rotenberg, N., le Feber, B., Visser, T.D., Kuipers, L., 2015. Tracking nanoscale electric and magnetic singularities through three-dimensional space. Optica 2 (6), 540–546. http://dx.doi.org/10.1364/OPTICA.2.000540.

Saghafi, S., Sheppard, C.J.R., 1998. Near field and far field of elegant Hermite-Gaussian and Laguerre-Gaussian modes. J. Modern Opt. 45 (10), 1999–2009. http://dx.doi.org/10.1080/09500349808231738.

Tkachuk, V.V., Korterik, J.P., Chang, L., Offerhaus, H.L., 2024. Sub-wavelength scale characterization of on-chip coupling mirrors. Opt. Express 32 (3), 2972. http://dx.doi.org/10.1364/OE.506358.

Tkachuk, V., Korterik, J., Offerhaus, H., 2023. Quantitative comparison of excitation modes of tuning forks for shear force in probe microscopy. Ultramicroscopy 253, 113772. http://dx.doi.org/10.1016/j.ultramic.2023.113772.

Zayats, A.V., Richards, D., 2009. Nano-Optics and Near-Field Optical Microscopy. In: Artech House Nanoscale Science and Engineering Series, Artech House.